

Silica-Coated Fe₃O₄ Nanoparticles as a Bifunctional Agent for Magnetic Resonance Imaging and ZnII Fluorescent Sensing

Technology in Cancer Research & Treatment
Volume 20: 1-9
© The Author(s) 2021
Article reuse guidelines:
sagepub.com/journals-permissions
DOI: 10.1177/15330338211036539
journals.sagepub.com/home/tct


Lin Qiu^{1,2}, Shuwen Zhou^{1,3}, Ying Li¹, Wen Rui¹, Pengfei Cui^{1,3},
Changli Zhang⁴, Yongsheng Yu⁵ , Cheng Wang^{1,3}, Xiang Wang³,
Jianhao Wang^{1,4,6} , and Pengju Jiang¹

Abstract

Bifunctional magnetic/fluorescent core-shell silica nanospheres (MNPs) encapsulated with the magnetic Fe₃O₄ core and a derivate of 8-aminoquinoline (N-(quinolin-8-yl)-2-(3-(triethoxysilyl) propylamino) acetamide) (QTEPA) into the shell were synthesized. These functional MNPs were prepared with a modified stöber method and the formed Fe₃O₄@SiO₂-QTEPA core-shell nanocomposites are biocompatible, water-dispersible, and stable. These prepared nanoparticles were characterized by X-ray power diffraction (XRD), transmission electron microscopy (TEM), thermoelectric plasma Quad II inductively coupled plasma mass spectrometry (ICP-MS), superconducting quantum interference device (SQUID), TG/DTA thermal analyzer (TGA) and Fourier transform infrared spectroscopy (FTIR). Further application of the nanoparticles in detecting Zn²⁺ was confirmed by the fluorescence experiment: the nanosensor shows high selectivity and sensitivity to Zn²⁺ with a 22-fold fluorescence emission enhancement in the presence of 10 μM Zn²⁺. Moreover, the transverse relaxivity measurements show that the core-shell MNPs have T2 relaxivity (r2) of 155.05 mM⁻¹ S⁻¹ based on Fe concentration on the 3.0 T scanner, suggesting that the compound can be used as a negative contrast agent for MRI. Further *in vivo* experiments showed that these MNPs could be used as MRI contrast agent. Therefore, the new nanosensor provides the dual modality of magnetic resonance imaging and optical imaging.

Keywords

nanosensor, Fe₃O₄ nanoparticles, magnetic resonance imaging, core-shell silica nanospheres, ZnII fluorescent sensing

Received: December 15, 2020; Revised: June 29, 2021; Accepted: June 30, 2021.

¹ School of Pharmacy & School of Medicine, Changzhou University, Changzhou, People's Republic of China

² Jiangsu Science Standard Medical Testing Co., Ltd, Changzhou, Jiangsu, People's Republic of China

³ The Affiliated Changzhou No. 2 People's Hospital of Nanjing Medical University, Changzhou, People's Republic of China

⁴ School of Environmental Science, Nanjing Xiaozhuang University, Nanjing, People's Republic of China

⁵ Clinical and Translational Research Center, Shanghai First Maternity and Infant Hospital, Tongji University School of Medicine, Shanghai, People's Republic of China

⁶ Changzhou Le Sun Pharmaceuticals Co., Ltd, Changzhou, Jiangsu, People's Republic of China

Corresponding Authors:

Xiang Wang, The Affiliated Changzhou No. 2 People's Hospital of Nanjing Medical University, Changzhou 213003, People's Republic of China.
Email: wx402@sohu.com

Jianhao Wang, School of Pharmacy & School of Medicine, Changzhou University, Changzhou 213164, People's Republic of China; School of Environmental Science, Nanjing Xiaozhuang University, Nanjing 211171, People's Republic of China; Changzhou Le Sun Pharmaceuticals Co., Ltd, Changzhou, Jiangsu 213125, People's Republic of China.
Email: minuswan@163.com

Pengju Jiang, School of Pharmacy & School of Medicine, Changzhou University, Changzhou 213164, People's Republic of China.
Email: pengju.jiang@gmail.com



Introduction

Compared with the dual-function molecular probes, the introduction of the nanoparticles makes more advantages of dual-function probes. In addition, as a new type of nanoparticles, magnetic fluorescent composite nanoparticles have attracted extensive attention in recent years. These composite nanoparticles take the advantages of molecular fluorescence, magnetic properties and nano-scaled materials, and can provide a potential platform for the construction of novel drugs for biological separation, targeting, biological imaging, tumor cell localization and even tumor therapy. Many interesting works have been reported based on these nanocomposites. Dual functional and multifunctional magnetic core shell $\text{Fe}_3\text{O}_4@\text{SiO}_2$ nanocomposites as a special carrier have attracted more and more attention.¹⁻⁶ The silica shell outside the iron oxide core not only increases the biocompatibility and stability of nanoparticles in water environment, but also provides convenient sites for modifying ligands in biomedical applications, such as biological separation,⁷⁻⁹ drug targeting,¹⁰⁻¹⁴ cell separation,⁸ enzyme immobilization¹⁵⁻¹⁸ and protein purification.¹⁹ In addition, $\text{Fe}_3\text{O}_4@\text{SiO}_2$ MNPs are more and more studied because they are easy to prepare and friendly to aqueous solution,²⁰ and can be designed into various shapes and sizes. On the other hand, some of which have been approved by FDA for clinical use. $\text{Fe}_3\text{O}_4@\text{SiO}_2$ NPs which have superparamagnetism have gradually become good drug agents, and FDA has approved the use of some of them in clinical practice.²¹ As a solid-state chemical sensor, sensor modified $\text{Fe}_3\text{O}_4@\text{SiO}_2$ nanoparticles have many attractive advantages in heterogeneous solid-liquid system. Such nanoparticles are easily obtained by hydrolysis reaction, meanwhile, different functional groups are introduced in the preparation process. For example, magnetic resonance contrast agents and fluorescent organic dyes can be constructed together into such nanoparticles, which produces a good platform for many potential applications.²⁰

A variety of transition metal ions play a wide range of roles in the environment and biological physiological processes.²²⁻²⁴ Among them, Zinc ions is the second most abundant transition metal ion in human body.^{25,26} In human body, most zinc are closely bound to enzymes and transcription factors,²⁷⁻³⁰ but many chelatable Zn(II) ions are still dissociated in certain cells and play important roles in biological systems.³¹⁻³⁸ In the human body, the brain is one of the organs with the highest zinc content. Studies showed that the concentration of free zinc ions in the brain is about 0.1-0.5 mM, and in the serum is about 12 μM . Zinc ions are components of many enzymes in human body. It is widely involved in cell proliferation and differentiation, nucleic acid and protein synthesis and many other important physiological activities.³⁹⁻⁴¹ Zinc ion is closely related to the central nervous system, for example, the decrease of zinc concentration in serum and plasma will increase the risk of Alzheimer's disease and Parkinson's disease.^{42,43} Therefore, intense research efforts have been devoted to the development of chemosensors for Zn^{2+} ion detection. Due to the unique role

of Zinc ions in physiological function, it is of great significance to detect and image Zinc ions in biological samples. In order to probe Zinc ions *in vivo* and *in vitro*, a large number of scientific researches have been carried out.⁴⁴ Among those reported Zn^{2+} sensors, quinoline derivatives are commonly chosen, such as 6-methoxy-(8-ptolunesulphonamido) quinoline (TSQ)⁴⁵ and its derivative (Zinquin series).⁴⁶⁻⁴⁸ These derivatives containing quinoline ring have been used for the fluorescence detection of zinc ions. It is obvious that the quinoline ring of supramolecular system, especially 8-aminoquinoline, has a very good selectivity for zinc ions.⁴⁹ However, some studies showed that zinc ion fluorescent probes containing quinoline ring have poor solubility in aqueous solution and are also interfered by other metal ions. In addition, many of the reported probes are difficult to work in the cellular environment. Therefore, there is still a great demand for the development of zinc ion fluorescent probes with wider versatility and higher performance.

With those concepts in mind, our strategy is to synthesize uniform dual-functionalized nanoparticles which permit dual-modality detections by incorporating organic fluorescent dye a chloroacetyl derivate of 8-aminoquinoline, N-(quinolin-8-yl)-2-(3-triethoxysilyl) propylamino) acetamide (QTEPA) into silica-coated magnetite core-shell (Figure 1). We utilized a common stöber method to synthesize the $\text{Fe}_3\text{O}_4@\text{SiO}_2$ silica-coated MNPs. However, Rastogi *et al*,⁵⁰ have reported the use of silica functional with the same fluorophore, QTEPA (Chemical structure shown in Figure S1), for the detection of Zn^{2+} . In our work, the difference is superparamagnetic Fe_3O_4 was added as the core. These QTEPA modified MNPs, as far as we known, are the first to be reported for not only exhibiting good selectivity and sensitivity for Zn^{2+} , but also of potential possibility to work as a T2 contrast agent.

Experimental

The experimental details were provided in the supporting information.

Results

Characterization of the Modification MNPs

The TEM image of magnetic Fe_3O_4 obtained in this study is shown in Figure 2 (left). The result showed that the shapes of Fe_3O_4 nanoparticles are nearly spherical, and the average particle size is about 7 nm.⁵¹ After the Fe_3O_4 NPs were modified with II, TEM revealed that the Fe_3O_4 were successfully encapsulated in silica shell, and the average particle size was about 20-30 nm as shown in Figure 2 (right). The TGA results indicated that the grafted ratio of onto $\text{Fe}_3\text{O}_4@\text{SiO}_2$ is about 10% (Figure S2).

The suspension prepared with Fe_3O_4 has good stability and can be kept for several months without obvious change. Dynamic light scattering (DLS) experiments showed that the hydrodynamic diameter of Fe_3O_4 NPs had almost no change in the first 2 months, and there was no obvious aggregation in 5 months. However, the stability $\text{Fe}_3\text{O}_4@\text{SiO}_2$ -QTEPA is

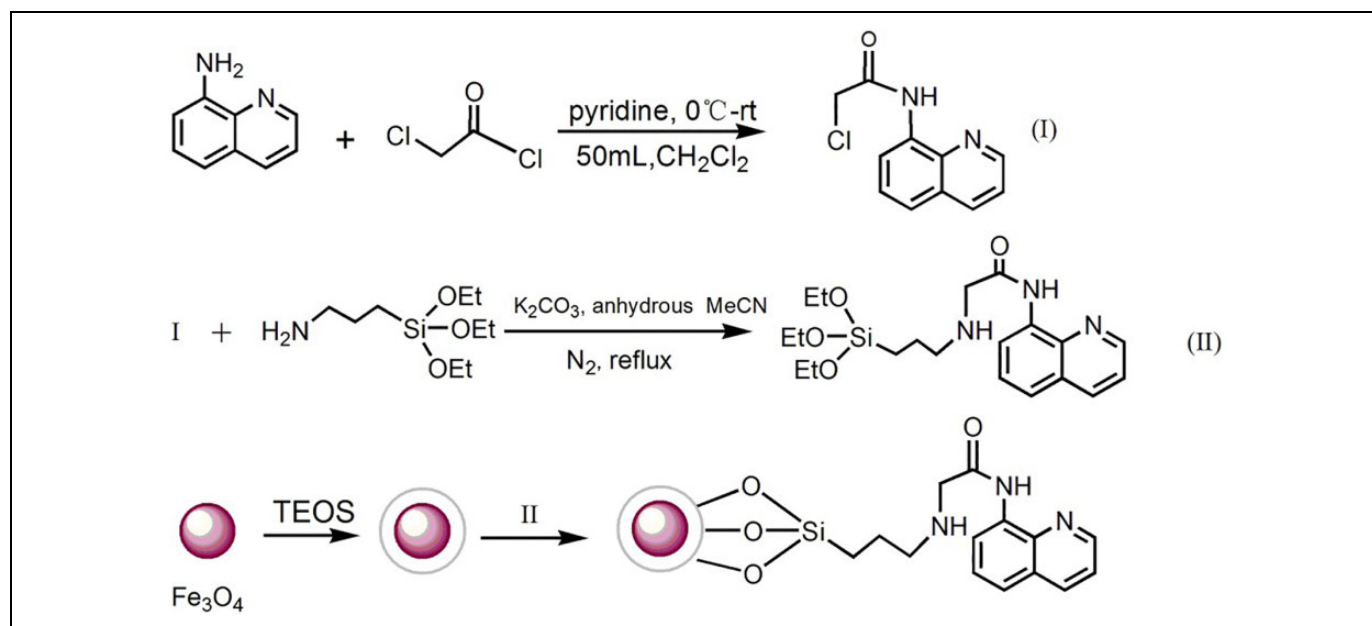


Figure 1. Schematic illustration of the formation of Fe₃O₄@SiO₂-QTEPA.

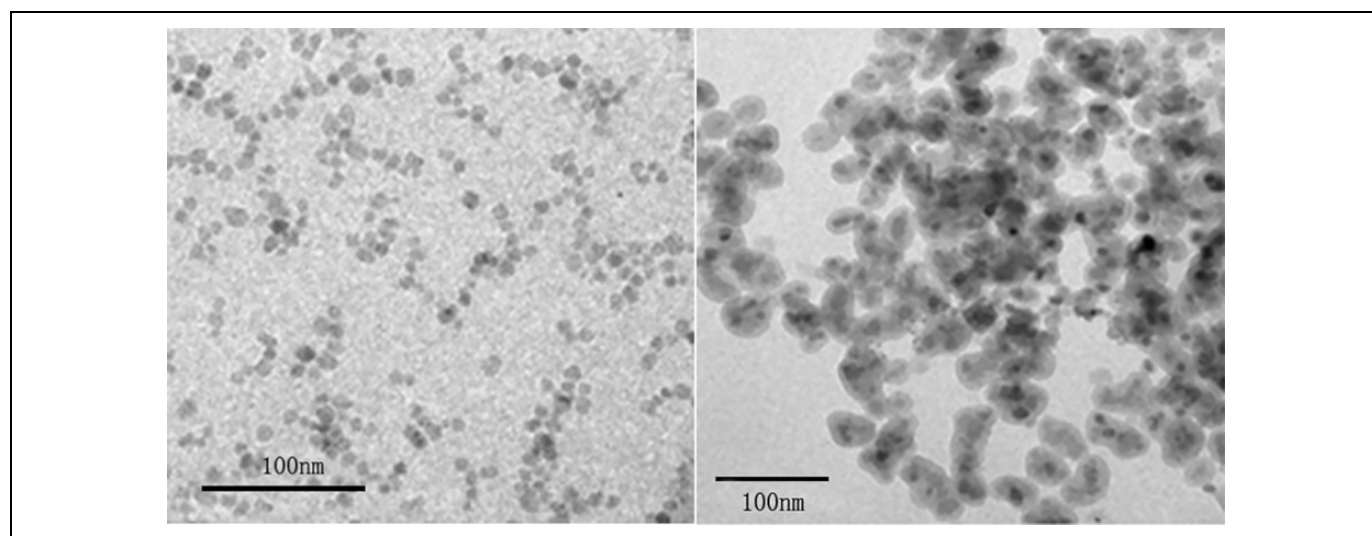


Figure 2. TEM images of Fe₃O₄ (left) and Fe₃O₄@SiO₂-QTEPA (right) (bar = 100 nm).

much less than pure Fe₃O₄, and the suspensions only maintain about 3-4 days (Figure S3).

Zeta potential (*Z*) reflects the degree of repulsion between adjacent, similarly charged particles in the dispersion. Particles with high *Z* (negative or positive) are electrically more stable than those with low *Z*, that is, the solution or dispersion of the former is more likely to resist aggregation. The zeta potential of Fe₃O₄ in aqueous solution is -18.8 mV, while Fe₃O₄@SiO₂-QTEPA aqueous solution has a net-negative charge at the value of -1.25 mV. Therefore, Fe₃O₄ NPs show higher water dispersibility than Fe₃O₄@SiO₂-QTEPA do. This is also a proof that the Fe₃O₄ was successfully grafted by SiO₂-QTEPA. This suggests that mutual repulsion between the macromolecules and subsequent lack of interactions.⁵²

The crystallographys of Fe₃O₄ and Fe₃O₄@SiO₂-QTEPA were verified by powder XRD (Figure 3). As shown in Figure 3, the diffraction patterns of both particles exhibit 6 peaks at 2θ of 30.1°, 35.5°, 43.1°, 53.6°, 57.2°, and 62.7° respectively, corresponding to standard inverse spinel phase of Fe₃O₄ (220) (311) (400) (422) (511) and (440) surface of the diffraction peak. The diffraction patterns and the relative intensities of all diffraction peaks of the 2 samples indicated that there were phases in both Fe₃O₄ and Fe₃O₄@SiO₂-QTEPA nanoparticles which are consistent with the crystal anti-spinel structure of magnetite (Fe₃O₄) and maghemite (γ-Fe₂O₃). The results also showed that the crystal Fe₃O₄ were encapsulated in the core-shell structure. Compared with the Fe₃O₄, all the diffraction peaks of Fe₃O₄@SiO₂-QTEPA are weakened, which due

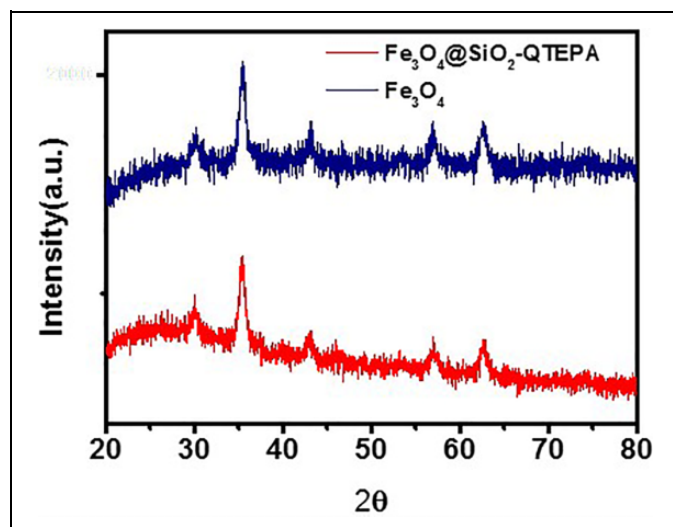


Figure 3. X-ray diffraction pattern of Fe_3O_4 and $\text{Fe}_3\text{O}_4@\text{SiO}_2\text{-QTEPA}$.

to the surface of silica and organic matter. And the broad peak between 20° and 25° (2θ) is assigned to the mesoporous silica oxide shell.

FTIR spectroscopy is used to confirm that QTEPA silicon is successfully immobilized on the $\text{Fe}_3\text{O}_4@\text{SiO}_2$ nanoparticles. The FT-IR spectra of $\text{Fe}_3\text{O}_4@\text{SiO}_2$ and $\text{Fe}_3\text{O}_4@\text{SiO}_2\text{-QTEPA}$ are shown in Figure 4. In Figure 4 (red line), the broad band centered at 3410.4 cm^{-1} represents silane and any form of water adsorbed on the surface of $\text{Fe}_3\text{O}_4@\text{SiO}_2$ nanoparticles. The band at 1643.3 cm^{-1} represents the bending mode of O-H vibrations. The strong band centered at 1103.04 cm^{-1} represents the structural Si-O-Si vibration, while the Si-OH vibration band appears in the $802\text{-}950\text{ cm}^{-1}$ region. Compared with the infrared spectrum of $\text{Fe}_3\text{O}_4@\text{SiO}_2$, the N-H stretching vibration band of $\text{Fe}_3\text{O}_4@\text{SiO}_2\text{-QTEPA}$ appears at 3402 cm^{-1} (black line) with the broad band of the silanol and moisture on the surface. The band at 1531.4 cm^{-1} is C = C aromatic stretching band, while the carbonyl band at 1662.3 cm^{-1} belongs to the aliphatic C-H stretching band. The FT-IR spectra clearly showed that II was successfully modified on the surface of MNPs.

Magnetic Properties $\text{Fe}_3\text{O}_4@\text{SiO}_2\text{-QTEPA}$

The magnetization curve of $\text{Fe}_3\text{O}_4@\text{SiO}_2\text{-QTEPA}$ is shown in Figure 5. The room temperature magnetization (m) curve of the samples with applied magnetic field (H) shows that the saturation magnetization (MS) is 15.2 emu/g . Due to the existence of core-shell structure, the room temperature magnetization $\text{Fe}_3\text{O}_4@\text{SiO}_2\text{-QTEPA}$ is lower than that of naked Fe_3O_4 nanoparticles (69.7 emu/g). Remanence and coercivity are almost invisible in the amplification curve (inset in Figure 5), which indicated that both nanoparticles have superparamagnetism at room temperature. So it can be considered that $\text{Fe}_3\text{O}_4@\text{SiO}_2\text{-QTEPA}$ NPs have enough magnetic attraction to effectively perform magnetic separation and can be used in nuclear magnetic resonance imaging.

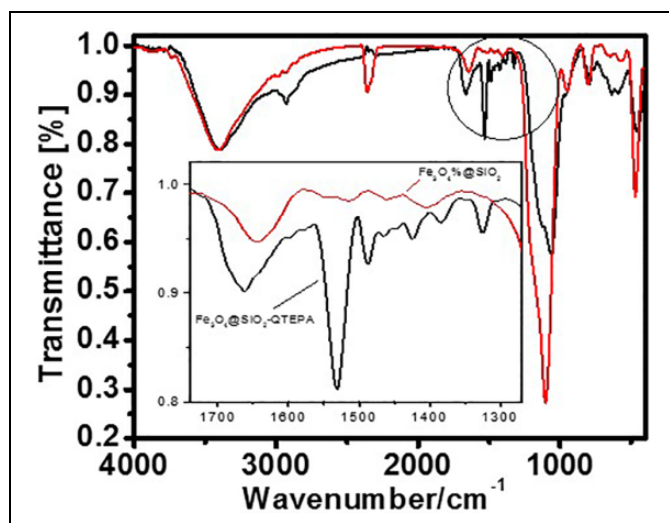


Figure 4. FTIR spectra of $\text{Fe}_3\text{O}_4@\text{SiO}_2$ (red line) and $\text{Fe}_3\text{O}_4@\text{SiO}_2\text{-QTEPA}$ (black line).

The superparamagnetism of magnetic NPs has a strong contrast effect on the surrounding tissues, which enables T_2 -weighted MRI to display tumor tissues in any plane of the body.^{53,54} Therefore, we measured the transverse relaxation time (T_2) to evaluate the negative-contrast effect of $\text{Fe}_3\text{O}_4@\text{SiO}_2\text{-QTEPA}$. In order to evaluate the performance and effect of $\text{Fe}_3\text{O}_4@\text{SiO}_2\text{-QTEPA}$ as T_2 contrast agent, we measured the transverse relaxation time (T_2) under 3 T magnetic field, and calculated the transverse relaxivity (r_2) according to the following equation⁵⁵:

$$1/T_2 = 1/T_2^0 + r_2 \cdot [Fe]$$

where T_2^0 is the standard relaxation time of pure water, $[Fe]$ is the concentration of Fe^{3+} calculated of $\text{Fe}_3\text{O}_4@\text{SiO}_2\text{-QTEPA}$ NPs (treated with nitric acid digestion). Each point in the Figure 6 is the transverse relaxation rate ($1/T_2$) of the solution at different concentrations, and the straight line is the linear relationship between the reciprocal of relaxation time and Fe^{3+} concentration. The linear fitting transverse relaxation rate is $155.05\text{ mM}^{-1}\text{ s}^{-1}$ (Figure 6), suggesting that the $\text{Fe}_3\text{O}_4@\text{SiO}_2\text{-QTEPA}$ NPs could be used as a T_2 -shortening agent to effectively relax the spin of water proton. These results showed that although Fe_3O_4 is coated by silica shell, it can still contact with water molecules, and the existence of shell structure only slightly affects the relaxation of Fe_3O_4 .

The T_2 -weighted magnetic resonance images of $\text{Fe}_3\text{O}_4@\text{SiO}_2\text{-QTEPA}$ in terms of different Fe concentrations are shown in Figure 7. The $\text{Fe}_3\text{O}_4@\text{SiO}_2\text{-QTEPA}$ NPs have good dispersion in water, which enabled us to detect the relaxivity of the particles in the solution at 3.0 T MR system. It is obvious from the Figure 7 that the $\text{Fe}_3\text{O}_4@\text{SiO}_2\text{-QTEPA}$ NPs displayed a signal enhancement in the T_2 weighted MRI image with the decrease of iron concentration, which means that MNPs may be used as the negative contrast agent of MRI.

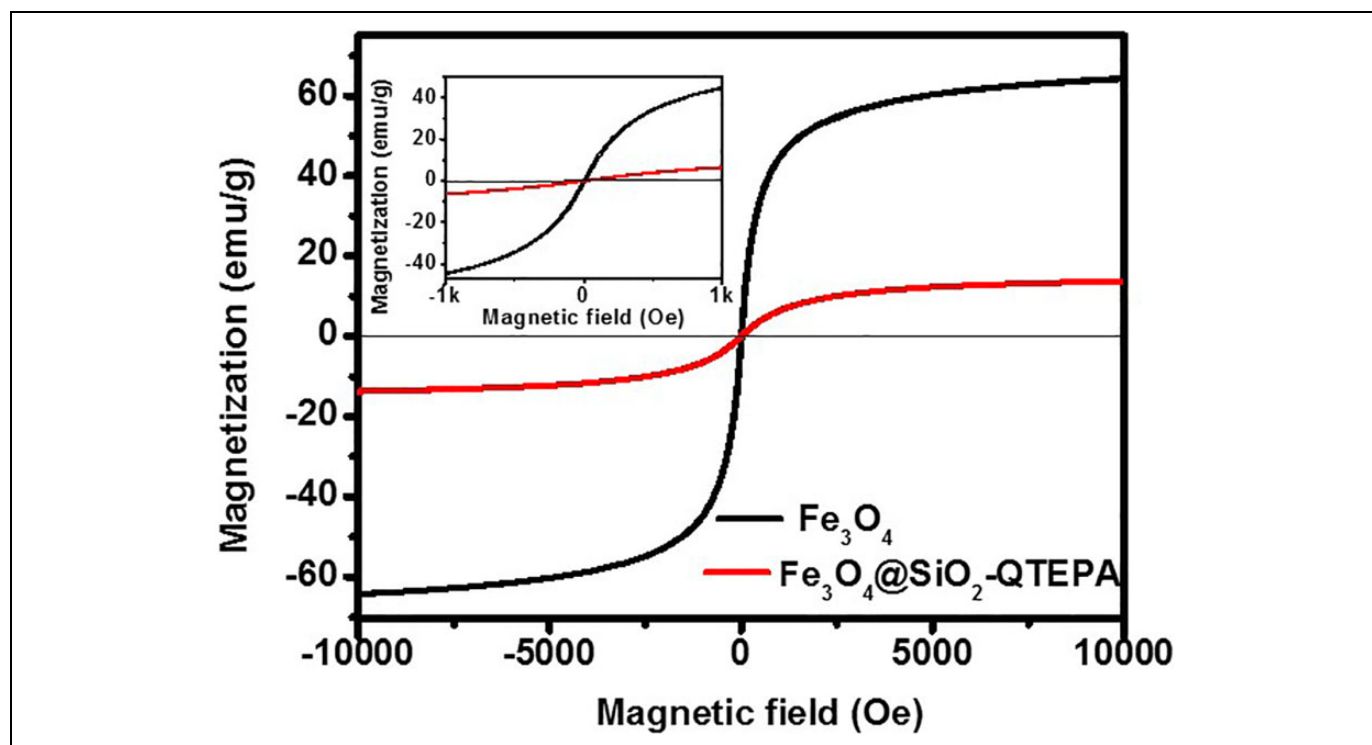


Figure 5. Room temperature magnetization curves of pure Fe_3O_4 powder and $\text{Fe}_3\text{O}_4@SiO_2$ -QTEPA.

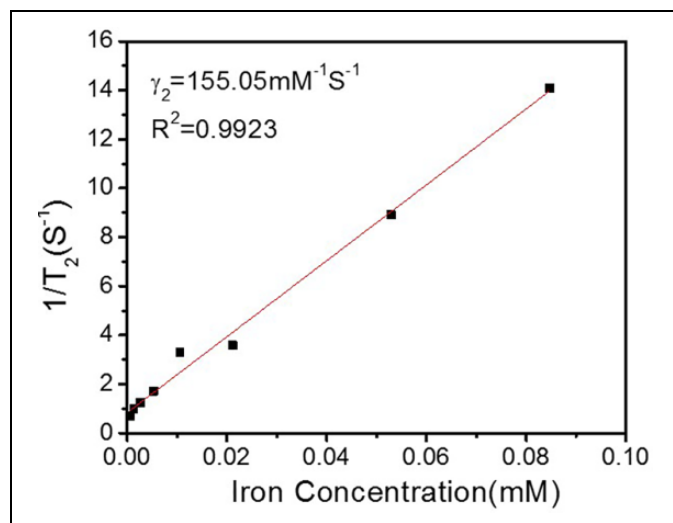


Figure 6. T_2 relaxivity plot of aqueous of $\text{Fe}_3\text{O}_4@SiO_2$ -QTEPA.

In Vitro and In Vivo MRI

The diagnostic potential of $\text{Fe}_3\text{O}_4@SiO_2$ -QTEPA was first explored *in vitro* by testing the negative-contrast effect in MCF-7 cells. To evaluate the possibility of using $\text{Fe}_3\text{O}_4@SiO_2$ -QTEPA nanoparticles as contrast agent to detect cancer cells, MCF-7 cells incubated with $\text{Fe}_3\text{O}_4@SiO_2$ -QTEPA nanoparticles suspension with different concentrations ($[\text{Fe}] = 0, 0.0025, 0.0050, 0.0075, 0.0100, 0.0125, 0.0150, 0.0175, 1.020,$

$0.0225, 0.025 \text{ mM}$) were detected by nuclear magnetic resonance (NMR). It can be clearly seen from the Figure 8 that the MR signal of MCF-7 cells treated by this method gradually decreased with the increase of Fe concentration. This suggested that $\text{Fe}_3\text{O}_4@SiO_2$ -QTEPA NPs have a good spatial resolution for T_2 MRI, which is consistent with the data reported in the literature based on iron oxide NPs.

Further, we carried out *in vivo* experiments. $\text{Fe}_3\text{O}_4@SiO_2$ -QTEPA suspension was injected into the mice via the tail vein and the changes of MR signal decline in the target organ liver were measured before and after injection (Figure 9A). The results showed that $\text{Fe}_3\text{O}_4@SiO_2$ -QTEPA accumulated in the normal liver, while no signal appeared in other organs, which confirmed that the MNPs eventually targeted and gathered in the liver. Figure 9A is an *in vivo* MRI image of mouse liver. Figure 9A shows the images of mice liver *in vivo* MRI. The images were acquired 1, 5, 7 and 12 h respectively after tail vein injection of the $\text{Fe}_3\text{O}_4@SiO_2$ -QTEPA suspension at 1 mg/mL $\text{Fe}_3\text{O}_4@SiO_2$ -QTEPA concentration, equivalent to a dose of 5 mg $\text{Fe}_3\text{O}_4@SiO_2$ -QTEPA/kg of the mice body weight, the color becomes darker after injection, and the signal cavity appears in the liver substance. The liver of mice was normal gray signal, while the signal becomes darker and darker after injection. After 1 h injection, the signal intensity in the liver decreased obviously. Compared with 5 and 7 hours after injection, 1 hour was the time that the MNPs accumulation in the normal liver arrived maximum value, and the MNPs gradually metabolized in the normal liver after 24 hours (Figure 9B).

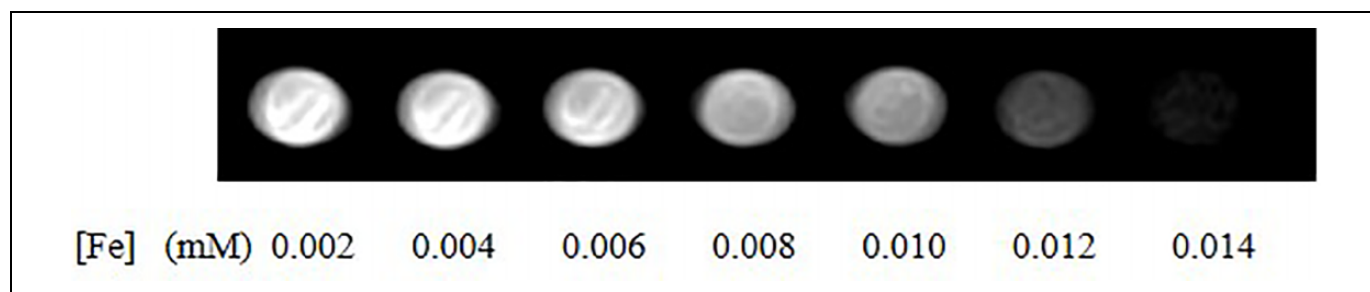


Figure 7. T₂-weighted MRI images of Fe₃O₄@SiO₂-QTEPA in water.

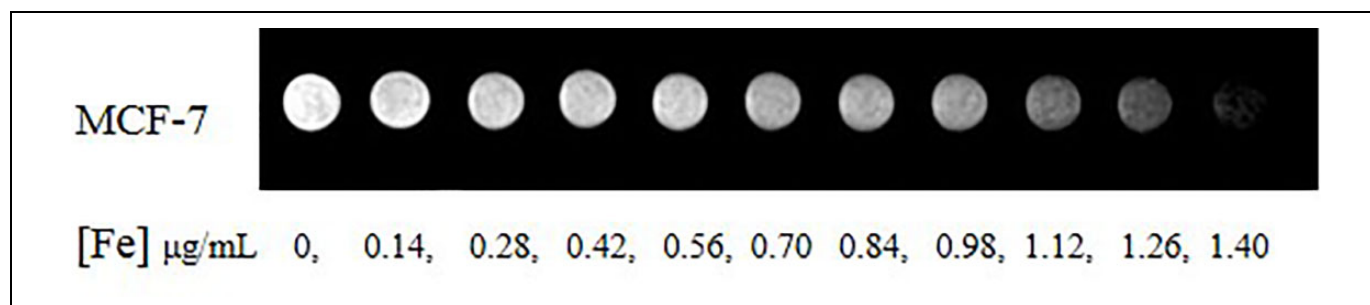


Figure 8. T₂-weighted MRI images of Fe₃O₄@SiO₂-QTEPA in MCF-7 cells for 3 h.

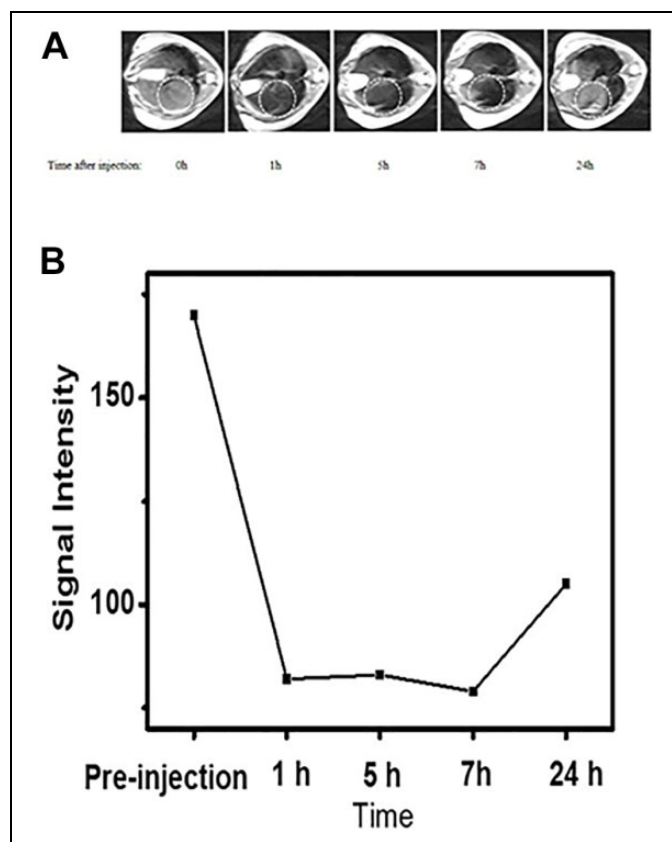


Figure 9. A, MR imaging of mouse liver regions after systemic administration of 150 μ L of Fe₃O₄@SiO₂-QTEPA (1 mg/mL). B, The time-dependent drop in MR T₂ signal intensities measured in the liver after the administration of Fe₃O₄@SiO₂-QTEPA.

Zn²⁺ Fluorescence Sensing

The fluorescence experiments of all metal ions were carried out in MNPs buffer solution (100 μ g of Fe₃O₄@SiO₂-QTEPA in 3 mL HEPES buffer). Fluorescence titration of Zn²⁺ was conducted using this suspension. Fe₃O₄@SiO₂-QTEPA showed a rather weak fluorescence signal in the range between 475 nm and 510 nm without Zn²⁺ ions. However, after adding Zn²⁺ to the concentration of 10 μ M, the fluorescence intensity of the solution increased by a factor of about 22 times at 490 nm, and the maximum emission shifted from 420 nm to 490 nm (Figure 10A). We also determined the fluorescence spectra the Fe₃O₄@SiO₂-QTEPA suspension in presence of Mn²⁺, Fe³⁺, Ag⁺, Cr³⁺, Co²⁺, Cu²⁺, Cd²⁺, Fe²⁺, Hg²⁺, Pb²⁺ and Ni²⁺. After adding these above metal ions to 20 μ M separately, the changes of fluorescence intensity at 490 nm are shown in Figure 10B. After adding different metal ions, only the addition of Hg²⁺ increased the fluorescence intensity slightly. Adding other metal ions to the Fe₃O₄@SiO₂-QTEPA suspension did not cause obvious change of fluorescence spectra. In addition, the enhancement of fluorescence intensity due to the addition of Zn²⁺ ions was not affected by the subsequent addition of other metal ions with concentrations of 20 μ M except K⁺, Ca²⁺, Na⁺, Mg²⁺ (200 μ M). (Figure S7 in the Supporting Information.)

We applied Fe₃O₄@SiO₂-QTEPA NPs for fluorescent imaging of Zn²⁺ in living cells to demonstrate the Fe₃O₄@SiO₂-QTEPA NPs with practical application potential in the buffer system. HeLa cells were incubated with Fe₃O₄@SiO₂-QTEPA NPs at 37°C for 4 h and washed thoroughly by PBS buffer to remove the extra Fe₃O₄@SiO₂-QTEPA NPs. Then with the

addition of Zn^{2+} , the living cells were incubated for another 20 minutes. The results showed that $Fe_3O_4@SiO_2$ -QTEPA NPs could penetrate the cell membrane for imaging Zn^{2+} in living cells, free $Fe_3O_4@SiO_2$ -QTEPA NPs in living cells showed

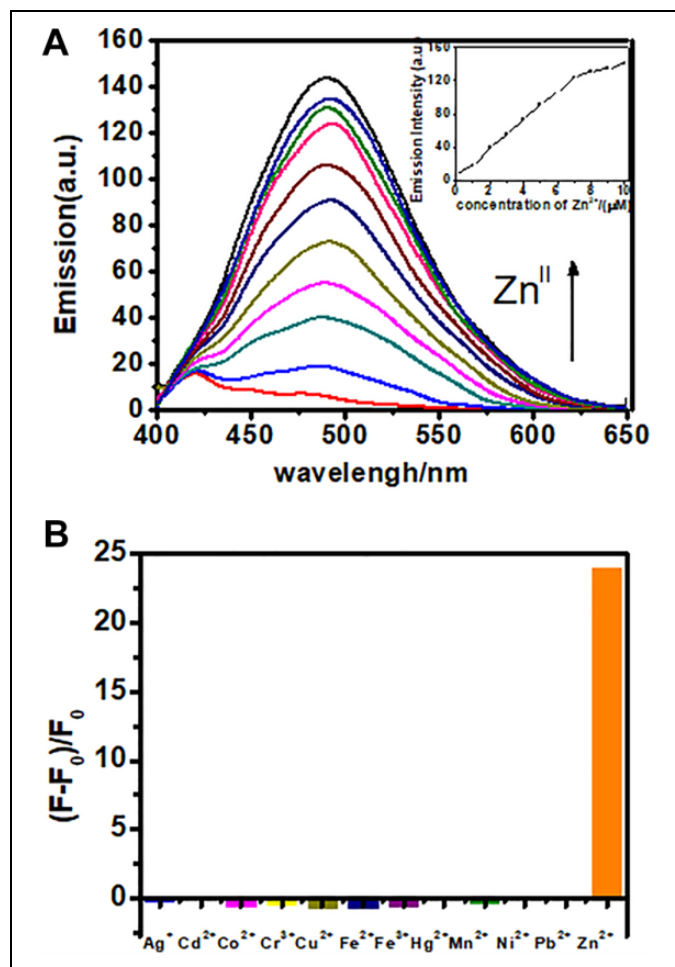


Figure 10. A, Fluorescence emission spectra of $Fe_3O_4@SiO_2$ -QTEPA (100 $\mu g/3$ mL) in the presence of Zn^{2+} from 1 μM to 10 μM in HEPES buffer. B, Bar graph of fluorescence emission intensity for 12 different metals showing metal selectivity profile of $Fe_3O_4@SiO_2$ -QTEPA in HEPES (5 mM, pH = 7.4) with the concentration of 20 μM for each metal.

very weak fluorescence (Figure 11B), a bright fluorescence was observed in the cells (Figure 11C) after adding Zn^{2+} in the above cells. Finally, TPEN (a good masking agent for Zn^{2+}) solution was added to the above cells for incubating another 20 minutes and fluorescence decreased (Figure 11D). These results demonstrated that $Fe_3O_4@SiO_2$ -QTEPA NPs can be applied for dual-mode *in vitro* imaging of Zn^{2+} ions in living cells and potentially sensitive *in vivo* MRI imaging as well. The comparison of Fe_3O_4 - SiO_2 -QTEPA with another similar materials in the literatures were summarized in Figure S4.

Conclusions

In summary, we demonstrate bifunctional nanoparticles based on silica-coated Fe_3O_4 MNPs which can be used as biocompatible magnetic T_2 MRI contrast agents and for imaging Zn^{2+} in living cells. To the best of our knowledge, these QTEPA functionalized MNPs are the first to be reported for not only exhibiting good selectivity and sensitivity for Zn^{2+} , but also of potential possibility to work as a T_2 contrast agent. This kind of core-shell magnetic nanoparticles has the comprehensive ability of fluorescence and MR imaging, and has the potential application for drug loading, which provides a platform for the research of targeting and biological imaging materials in biological systems. These results provide considerable foundation and reference for the construction of bifunctional magnetic nanoparticles. The magnetic nanoparticles modified by appropriate fluorescent probe molecules have good biocompatibility and can be used in fluorescence imaging and nuclear magnetic resonance imaging.

Authors' Note

The use of the animal in current study was approved by the Ethics Board of Tongji University School of Medicine. Approval number KS18183.

Acknowledgments

We thank the Jiangsu Key Research and Development Plan (Society Development, No. BE2018639), Science & Technology Support Program of Changzhou (Application Basic Research CJ20190033), Natural Science Foundation of Jiangsu (grant number BK20190566) and

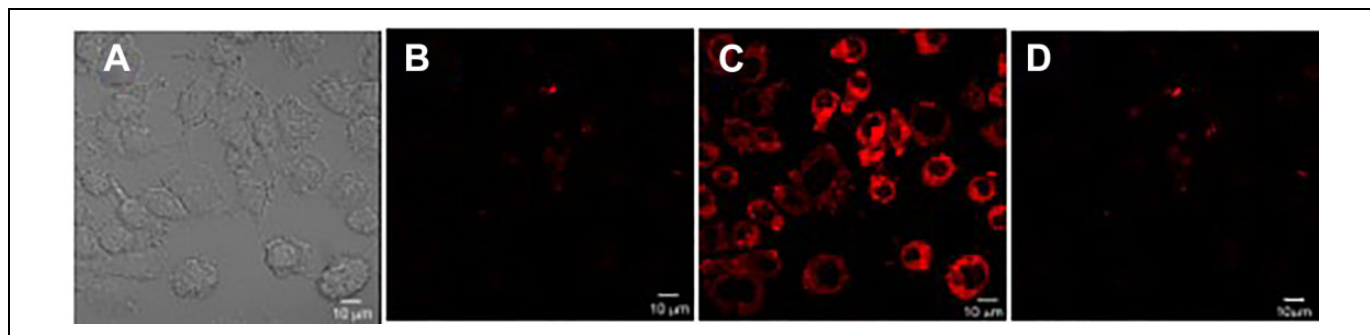


Figure 11. Bright image (A) and fluorescence images of HeLa cells incubated with $Fe_3O_4@SiO_2$ -QTEPA NPs in the absence (B) and presence (C) of Zn^{2+} , and TPEN was added to eliminate Zn^{2+} (D). Scale bar is 10 μm .

the International Scientific Cooperation Project of Changzhou Scientific Bureau (grant numbers CZ20190004, CZ20190009). This work was also supported by The Qing Lan Project of Jiangsu Province.

Declaration of Conflicting Interests

The author(s) declared no potential conflicts of interest with respect to the research, authorship, and/or publication of this article.

Funding

The author(s) disclosed receipt of the following financial support for the research, authorship, and/or publication of this article: The Jiangsu Key Research and Development Plan (Society Development, No. BE2018639), Science & Technology Support Program of Changzhou (Application Basic Research CJ20190033), Natural Science Foundation of Jiangsu (grant number BK20190566) and the International Scientific Cooperation Project of Changzhou Scientific Bureau (grant numbers CZ20190004, CZ20190009).

ORCID iDs

Yongsheng Yu  <https://orcid.org/0000-0001-5139-3439>

Jianhao Wang  <https://orcid.org/0000-0003-3133-6132>

Supplemental Material

Supplemental material for this article is available online.

References

- Jiang W, Wu L, Duan J. Ultrasensitive electrochemiluminescence immunosensor for 5-hydroxymethylcytosine detection based on Fe₃O₄@SiO₂ nanoparticles and PAMAM dendrimers. *Biosens Bioelectron.* 2018;99:660-666. doi:10.1016/j.bios.2017.08.023
- Zasonska BA, Boiko N, Horak D, et al. The use of hydrophilic poly (N, N-dimethylacrylamide) for promoting engulfment of magnetic gamma-Fe₂O₃ nanoparticles by mammalian cells. *J Biomed Nanotechnol.* 2013;9(3):479-491. doi:10.1166/jbn.2013.1552
- Li Z, Zheng Y, Gao T, et al. Fabrication of biosensor based on core-shell and large void structured magnetic mesoporous microspheres immobilized with laccase for dopamine detection. *J Mater Sci.* 2018;53(11):7996-8008. doi:10.1007/s10853-018-2165-z
- Furlan PY, Furlan AY, Kisslinger K, et al. Water as the solvent in the stober process for forming ultrafine silica shells on magnetite nanoparticles. *ACS Sustainable Chem Eng.* 2019;7(18):15578-15584. doi:10.1021/acssuschemeng.9b03554
- Shen L, Li B, Qiao Y. Monodisperse Fe₃O₄/SiO₂ and Fe₃O₄/SiO₂/PPy core-shell composite nanospheres for IBU loading and release. *Materials (Basel).* 2019;12(5):828. doi:10.3390/ma12050828
- Su Y, Shao C, Huang X, et al. Extraction and detection of bisphenol A in human serum and urine by aptamer-functionalized magnetic nanoparticles. *Anal Bioanal Chem.* 2018;410(7):1885-1891. doi:10.1007/s00216-017-0801-0
- Zhao Q, Wu Q, Ma P, et al. Selective and sensitive fluorescence detection method for pig IgG based on competitive immunosensing strategy and magnetic bioseparation. *Talanta.* 2019;195:103-108. doi:10.1016/j.talanta.2018.11.041
- Mostafaei M, Hosseini SN, Khatami M, Javidanbardan A, Sepahy AA, Asadi E. Isolation of recombinant Hepatitis B surface antigen with antibody-conjugated superparamagnetic Fe₃O₄/SiO₂ core-shell nanoparticles. *Protein Expr Purif.* 2018;145:1-6. doi:10.1016/j.pep.2017.12.004
- Lee DW, Fatima H, Kim KS. Preparation of silica coated magnetic nanoparticles for bioseparation. *J Nanosci Nanotechnol.* 2018;18(2):1414-1418. doi:10.1166/jnn.2018.14888
- Liu C, Yang B, Chen X, et al. Capture and separation of circulating tumor cells using functionalized magnetic nanocomposites with simultaneous in situ chemotherapy. *Nanotechnology.* 2019;30(28):285706. doi:10.1088/1361-6528/ab0e25
- Liu Y, Yang K, Cheng L, et al. PEGylated FePt@Fe₂O₃ core-shell magnetic nanoparticles: potential theranostic applications and in vivo toxicity studies. *Nanomedicine.* 2013;9(7):1077-1088. doi:10.1016/j.nano.2013.02.010
- Yang Y, Fan H, Xie J. Facile preparation of multifunctional Fe₃O₄@SiO₂@LaVO₄:Eu³⁺ nanocomposites as potential drug carriers. *Ceramics International.* 2016;42(16):19445-19449. doi:10.1016/j.ceramint.2016.09.098
- Tang Y, Zhao H, Yao J. A doxorubicin and vincristine drug release system based on magnetic PLGA microspheres prepared by coaxial electrospray. *J Mater Sci.* 2019;54:9689-9706. doi:10.1007/s10853-019-03575-9
- Pourmanouchehri Z, Jafarzadeh M, Kakaei S, Khameneh ES. Magnetic nanocarrier containing Ga-68-DTPA complex for targeted delivery of doxorubicin. *J Inorg Organomet Polym Mater.* 2018;28(5):1980-1990. doi:10.1007/s10904-018-0826-7
- Jiang XP, Lu TT, Liu CH, et al. Immobilization of dehydrogenase onto epoxy-functionalized nanoparticles for synthesis of (R)-mandelic acid. *Int J Biol Macromol.* 2016;88:9-17. doi:10.1016/j.ijbiomac.2016.03.031
- Jaquish R, Reilly AK, Lawson BP, et al. Immobilized glucose oxidase on magnetic silica and alumina: beyond magnetic separation. *Int J Biol Macromol.* 2018;120:896-905. doi:10.1016/j.ijbiomac.2018.08.097
- Cui J, Sun B, Lin T, Feng Y, Jia S. Enzyme shielding by mesoporous organosilica shell on Fe₃O₄@silica yolk-shell nanospheres. *Int J Biol Macromol.* 2018;117:673-682. doi:10.1016/j.ijbiomac.2018.05.227
- Aslani E, Abri A, Pazhang M. Immobilization of trypsin onto Fe₃O₄@SiO₂-NH₂ and study of its activity and stability. *Colloid Surface B.* 2018;170:553-562. doi:10.1016/j.colsurfb.2018.06.022
- Chang M, Qin Q, Wang B, et al. Carboxymethylated polyethylenimine modified magnetic nanoparticles specifically for purification of His-tagged protein. *J Sep Sci.* 2019;42(3):744-753. doi:10.1002/jssc.201800969
- Chatterjee S, Li XS, Liang F. Design of multifunctional fluorescent hybrid materials based on SiO₂ materials and core-shell Fe₃O₄@SiO₂ nanoparticles for metal ion sensing. *Small.* 2019;15(44):1904569. doi:10.1002/sml.201904569
- Veisheh O, Gunn JW, Zhang M. Design and fabrication of magnetic nanoparticles for targeted drug delivery and imaging. *Adv Drug Deliv Rev.* 2010;62(3):284-304. doi:10.1016/j.addr.2009.11.002
- Zheng HL, Youdim MBH, Weiner LM. Novel potential neuroprotective agents with both iron chelating and amino acid-based derivatives targeting central nervous system neurons. *Biochem Pharmacol.* 2005;70(11):1642-1652. doi:10.1016/j.bcp.2005.09.003

23. Viles JH. Metal ions and amyloid fiber formation in neurodegenerative diseases. Copper, zinc and iron in Alzheimer's, Parkinson's and prion diseases. *Coordin Chem Rev.* 2012;256(19-20):2271-2284. doi:10.1016/j.ccr.2012.05.003
24. Bonda DJ, Lee HG, Blair JA, Zhu X, Perry G, Smith MA. Role of metal dyshomeostasis in Alzheimer's disease. *Metallomics.* 2011;3(3):267-270. doi:10.1039/c0mt00074d
25. Parker MM, Humoller FL, Mahler DJ. Determination of copper and zinc in biological material. *Clin Chem.* 1967;13(1):40-48.
26. Bush AI. Metals and neuroscience. *Curr Opin Chem Biol.* 2000;4(2):184-191. doi:10.1016/s1367-5931(99)00073-3
27. Cox EH, McLendon GL. Zinc-dependent protein folding. *Curr Opin Chem Biol.* 2000;4(2):162-165. doi:10.1016/s1367-5931(99)00070-8
28. Berg JM, Shi Y. The galvanization of biology: a growing appreciation for the roles of zinc. *Science.* 1996;271(5252):1081-1085. doi:10.1126/science.271.5252.1081
29. Clarke ND, Berg JM. Zinc fingers in *Caenorhabditis elegans*: finding families and probing pathways. *Science.* 1998;282(5396):2018-2022. doi:10.1126/science.282.5396.2018
30. Jiang PJ, Guo ZJ. Fluorescent detection of zinc in biological systems: recent development on the design of chemosensors and biosensors. *Coordin Chem Rev.* 2004;248(1-2):205-229. doi:10.1016/j.ccr.2003.10.013
31. Zhang J, Campbell RE, Ting AY. Creating new fluorescent probes for cell biology. *Nat Rev Mol Cell Biol.* 2003;4. doi:10.1038/nrm1031
32. Lim NC, Yao L, Freake HC, et al. Synthesis of a fluorescent chemosensor suitable for the imaging of Zinc(II) in live cells. *Bioorg Med Chem Lett.* 2003;13(14):2251-2254. doi:10.1016/s0960-894x(03)00464-5
33. Chang CJ, Nolan EM, Jaworski J. Bright fluorescent chemosensor platforms for imaging endogenous pools of neuronal zinc. *Chem Biol.* 2004;11(2):203-210. doi:10.1016/j.chembiol.2004.01.017
34. Frederickson CJ, Suh SW, Silva D. Importance of zinc in the central nervous system: the zinc-containing neuron. *J Nutr.* 2000;130(5S Suppl):1471S-1483S.
35. Kay AR. Evidence for chelatable zinc in the extracellular space of the hippocampus, but little evidence for synaptic release of Zn. *J Neurosci.* 2003;23(17):6847-6855.
36. Cole TB, Martyanova A, Palmiter RD. Removing zinc from synaptic vesicles does not impair spatial learning, memory, or sensorimotor functions in the mouse. *Brain Res.* 2001;891(1-2):253-265. doi:10.1016/s0006-8993(00)03220-0
37. Lee JY, Cole TB, Palmiter RD. Accumulation of zinc in degenerating hippocampal neurons of ZnT3-null mice after seizures: evidence against synaptic vesicle origin. *J Neurosci.* 2000;20(11):79. doi:10.1523/JNEUROSCI.20-11-j0003.2000
38. Kikuchi K, Komatsu K, Nagano T. Zinc sensing for cellular application. *Curr Opin Chem Biol.* 2004;8(2):182-191. doi:10.1016/j.cbpa.2004.02.007
39. Outten CE, O'Halloran TV. Femtomolar sensitivity of metalloregulatory proteins controlling zinc homeostasis. *Science.* 2001;292(5526):2488-2492. doi:10.1126/science.1060331
40. Lopez-Garcia C, Varea E, Palop JJ, et al. Cytochemical techniques for zinc and heavy metals localization in nerve cells. *Microsc Res Tech.* 2002;56(5):318-331. doi:10.1002/jemt.10037
41. Finney LA, O'Halloran TV. Transition metal speciation in the cell: insights from the chemistry of metal ion receptors. *Science.* 2003;300(5621):931-936. doi:10.1126/science.1085049
42. Majewski M, Kozłowska A, Thoene M. Overview of the role of vitamins and minerals on the kynurenine pathway in health and disease. *J Physiol Pharmacol.* 2016;67(1):3-19.
43. Isaev NK, Stelmashook EV, Genrikhs EE. Role of zinc and copper ions in the pathogenetic mechanisms of traumatic brain injury and Alzheimer's disease. *Rev Neurosci.* 2020;31(3):233-243. doi:10.1515/revneuro-2019-0052
44. Li J, Yin C, Huo F. Development of fluorescent zinc chemosensors based on various fluorophores and their applications in zinc recognition. *Dyes Pigm.* 2016;131:100-133. doi:10.1016/j.dyepig.2016.03.043
45. Frederickson CJ, Kasarskis EJ, Ringo D. A quinoline fluorescence method for visualizing and assaying the histochemically reactive zinc (bouton zinc) in the brain. *J Neurosci Methods.* 1987;20(2):91-103. doi:10.1016/0165-0270(87)90042-2
46. Zalewski PD, Forbes IJ, Betts WH. Correlation of apoptosis with change in intracellular labile Zn(II) using zinquin [(2-methyl-8-p-toluenesulphonamido-6-quinolyloxy)acetic acid], a new specific fluorescent probe for Zn(II). *Biochem.* 1993;296(Pt 2)(Pt 2):403-408. doi:10.1042/bj2960403
47. Zalewski PD, Forbes IJ, Seamark RF. Flux of intracellular labile zinc during apoptosis (gene-directed cell death) revealed by a specific chemical probe, Zinquin. *Chem Biol.* 1994;1(3):153-161. doi:10.1016/1074-5521(94)90005-1
48. Mahadevan IB, Kimber MC, Lincoln SF, et al. The synthesis of Zinquin ester and Zinquin acid, zinc(II)-specific fluorescing agents for use in the study of biological zinc(II). *Aust J Chem.* 1996;49(5):561-568. doi:10.1071/ch9960561
49. Pearce DA, Jotterand N, Carrico IS. Derivatives of 8-hydroxy-2-methylquinoline are powerful prototypes for zinc sensors in biological systems. *J Am Chem Soc* 2001;123(21):5160-5161. doi:10.1021/ja0039839
50. Rastogi SK, Pal P, Aston DE. 8-Aminoquinoline functionalized silica nanoparticles: a fluorescent nanosensor for detection of divalent zinc in aqueous and in yeast cell suspension. *ACS Appl Mater Interfaces.* 2011;3(5):1731-1739. doi:10.1021/am2002394
51. Qu H, Caruntu D, Liu H. Water-dispersible iron oxide magnetic nanoparticles with versatile surface functionalities. *Langmuir.* 2011;27(6):2271-2278. doi:10.1021/la104471r
52. Sohn GJ, Choi HJ, Jeon IY. Water-dispersible, sulfonated hyperbranched poly(ether-ketone) grafted multiwalled carbon nanotubes as oxygen reduction catalysts. *ACS Nano.* 2012;6(7):6345-6355. doi:10.1021/nn301863d
53. Park JH, von Maltzahn G, Zhang L, et al. Magnetic iron oxide nanoworms for tumor targeting and imaging. *Adv Mater.* 2008;20(9):1630. doi:10.1002/adma.200800004
54. Sailor MJ, Park JH. Hybrid Nanoparticles for detection and treatment of cancer. *Adv Mater.* 2012;24(29):3779-3802. doi:10.1002/adma.201200653
55. Yang H, Zhang C, Shi X, et al. Water-soluble superparamagnetic manganese ferrite nanoparticles for magnetic resonance imaging. *Biomaterials.* 2010;31(13):3667-3673. doi:10.1016/j.biomaterials.2010.01.055